Hierarchical Tuning of the Performance of Electrochemical Carbon Dioxide Reduction Using Conductive Two-Dimensional Metallophthalocyanine Based Metal–Organic Frameworks

Zheng Meng,[1†] Jianmin Luo,[2†] Weiyang Li,[2*] and Katherine A. Mirica[1*]

[1]Department of Chemistry, Dartmouth College, Hanover, New Hampshire 03755, USA.

[2]Thayer School of Engineering, Dartmouth College, Hanover, New Hampshire 03755, USA.

ABSTRACT: The use of reticular materials in the electrochemical reduction of carbon dioxide to value-added products has the potential to enable tunable control of the catalytic performance through the modulation of chemical and structural features of framework materials with atomic precision. However, the tunable functional performance of such systems is still largely hampered by their poor electrical conductivities. This paper demonstrates the use of four systematic structural analogs of conductive two-dimensional (2D) metal–organic frameworks (MOFs) made of metallophthalocyanine (MPc) ligands linked by Cu nodes with electrical conductivities of 2.73×10^{-3} to 1.04×10^{-1} S cm^{-1} for the electrochemical reduction of CO_2 to CO. The catalytic performance of the MOFs, including the activity and selectivity, is found to be hierarchically governed by two important structural factors: the metal within the MPc (M=Co vs Ni) catalytic subunit and the identity of the heteroatomic crosslinkers between these subunits (X=O vs NH). The activity and selectivity are dominated by the choice of metal within MPcs and are further modulated by the heteroatomic linkages. Among these MOFs, **CoPc-Cu-O** exhibited the highest selectivity toward CO product (Faradic efficiency FE_{CO}=85%) with high current densities up to −17.3 mA cm^{-2} as a composite with carbon black at 1:1 mass ratio) at a low overpotential of −0.63 V. Without using any conductive additives, the use of **CoPc-Cu-O** directly as an electrode material was able to achieve a current density of −9.5 mA cm^{-2} with a FE_{CO} of 79%. Mechanistic studies by comparison tests with metal-free phthalocyanine MOF analogs supported the dominant catalytic role of the central metal of the phthalocyanine over Cu nodes. Density-functional theory (DFT) calculations further suggested that, compared with the NiPc-based and NH-linked analogs, CoPc-based and O-linked MOFs have lower activation energies in the formation of carboxyl intermediate, in line with their higher activities and selectivity. The results of this study indicate that the use of 2D MPc-based conductive framework materials holds great promise for achieving efficient CO_2 reduction through strategic ligand engineering with multiple levels of tunability.

INTRODUCTION

Electrochemical reduction of carbon dioxide (CO_2) to value-added carbon source carbon monoxide (CO), represents an important pathway for recycling combustion products into fuels and providing an avenue towards carbon-neutral economy.[1-4] Efforts toward the effective and selective electrochemical reduction of CO_2 to CO have led to the development of various homogeneous and heterogeneous catalysts.[3-8] Homogeneous molecular catalysts, mainly represented by metal coordination complexes, can achieve high energy efficiency (low overpotential) and selectivity by the systematic tuning of their molecular structures through the strategic choice of coordination metals or appropriate functionalization of organic ligands.[5, 7, 9-14] However, molecular catalysts often lack high catalytic activity (as evidenced by low current density) because of catalyst deactivation and inefficient electron transfers between multiple components in solution, and they often require organic media for optimal selectivity and stability.[2, 12, 15-17] Heterogeneous catalysts, including metals,[18-19] metal oxides,[20-21] metal chalcogenides,[22-24] graphene,[25-27]polymers,[28-30] and a series of composite materials consisting of metals,[13, 31] graphene,[32-35] and carbon nanotubes,[32, 36-37] are attractive alternatives, as they can offer high conductivity and aqueous compatibility with the ability to provide good catalytic activity. However, rational control of activity and selectivity at the molecular level is difficult to achieve for many heterogeneous catalysts.[38] To date, the most successful systems rely mainly on the use of noble metals, such as Au, Ag, and Pd, which are cost-prohibitive at large scale because of their rarity.[39-43] Thus, the development of novel nanomaterials comprising earth-abundant non-noble chemical elements capable of promoting electrocatalytic reduction of CO_2 to CO with high energy-efficiency, activity, and selectivity, as well as possessing well-defined and tailorable structures for tuning the structure–property–performance relationship is in high demand.

Reticular materials,[44-47] including metal–organic frameworks (MOFs) and covalent organic frameworks (COFs), which can be built from modular organic linkers and inorganic metal/cluster nodes, represent a unique class of solid-state materials that have straightforward accessibility, chemical stability, structural regularity, and extreme tunability at the molecular level.[48-51] The bottom-up self-assembly of reticular materials enables precise manipulation and controlled spatial arrangement of molecular catalysts within a framework architecture necessary for tunable

activity and selectivity,[52-53] while their high surface areas and intrinsic porosities can permit access of reactants to active sites.[54-55] Therefore, reticular materials represent a privileged class of solid-state catalysts, which can combine the beneficial features from both homogeneous and heterogeneous catalysts, such as well-defined structure, tailorable properties, intrinsic conductivity, and chemical stability.

While several precedents currently exist for utilizing MOFs and COFs for CO_2 reduction to CO,[49, 56-64] with few exceptions,[59, 65] the existing approaches mostly rely on frameworks with low conductivities, and consequently lead to low current densities (<5 mA cm^{-2}).[49, 56-58, 60-62, 64] The recent emergence of conductive MOFs and COFs offers the possibility to overcome these issues by enhancing the through-bond and through-space charge transport within a framework *via* the utilization of redox-active building blocks, the construction of d-π or π-π conjugated structures, and the formation of π-stackings.[66-72] While several recent approaches employing conductive framework materials to facilitate CO_2 reduction to CO highlight the potential utility of this class of materials,[59, 63, 65] the fundamental understanding of how different structural features on the molecular level contribute to selectivity and catalytic efficiency remains limited. Moreover, despite this encouraging progress, the potential of conductive framework materials for achieving high current density without the assistance of conductive additives remains unexplored. Importantly, the demonstration of using a series of isoreticular conductive frameworks for systematic tuning of the efficiency and selectivity of electrochemical CO_2 reduction through a ligand engineering strategy remains unprecedented. Thus, encouraged by several recent reports,[59, 63, 65] we reasoned that the systematic structural modulation of a conductive MOF system can allow fundamental investigation of multiple levels of control over the interplay between catalytic efficiency, activity, and selectivity within an isoreticular MOF system.[66-67]

This paper focuses on the use of four systematic isoreticular structural analogs of 2D conductive MOFs (**Scheme 1**), including **CoPc-Cu-NH**, **CoPc-Cu-O**, **NiPc-Cu-NH**, and **NiPc-Cu-O,** as electrocatalysts in the electrochemical reduction of CO_2 that permit the modulation of the efficiency, activity, and selectivity. These four MOFs share the same P4/mmm lattice with square pore apertures of 1.8 nm with large surface-to-volume ratios and Brunauer-Emmett-Teller surface area of 349–628 m^2 g^{-1}, good CO_2 adsorption ability of 1.48–2.03 mmol g^{-1} (900 Torr, 298 K), and good electrical conductivities in the range of 2.73×10^{-3} to 1.04×10^{-1} S cm^{-1}. Cathodes based on MOFs and carbon black (CB) deposited on carbon fibers showed for the first time that these four MOFs are able to catalyze the CO_2 to CO conversion with high activities with current densities (j) of –6.1 to –21.8 mA cm^{-2} at the potential of –0.74 to –0.94 V (overpotential η, –0.63 to –0.83 V), and are stable during the electrochemical process. We demonstrate that the catalytic performance of the MOFs, including the product distribution and activity, is governed by the choice of two important structural features within this class of materials: the metal within the MPc catalytic subunit (M=Co vs Ni) and the identity of the heteroatomic crosslinkers between these subunits (X=O vs NH). These two features enabled a hierarchical tuning of the CO_2 reduction performance, in which the activity and selectivity are dominated by the choice of metal of MPcs and are further modulated by heteroatomic linkages. Electrochemical tests using metal-free phthalocyanine controls **Pc-Cu-X** (**Pc-Cu-O** and **Pc-Cu-NH, Scheme S8**) supported the essential role of the central metal within the phthalocyanine cavity in the catalytic CO_2 to CO transformation. Through computational studies, we uncovered that compared with the NiPc-based and NH-linked analogs, CoPc-based and O-linked MOFs have lower activation energies for the formation of carboxyl intermediate, which may explain their higher activities and selectivity.

Among the MOFs examined, **CoPc-Cu-O** exhibited the highest selectivity toward CO product (FE_{CO}=85%) with high current densities (j=–13.1 and –17.3 mA cm^{-2} for **CoPc-Cu-O**/CB in mass ratio of 1:0.5 and 1:1, respectively) at a relatively low overpotential of –0.63 V, which is among one of best cathode materials for the catalytic electrochemical conversion of CO_2 to CO using reticular materials (**Table S11**). Without using conductive additive CB, **CoPc-Cu-O** directly deposited on to carbon fiber electrodes was able to achieve a high FE_{CO} of 79% with a current density of –9.5 mA cm^{-2} at a relatively low overpotential of –0.63 V. Our results suggest that, compared with their 3D counterparts, 2D MPc-based conductive MOFs also hold great promise for achieving efficient CO_2 reduction.

MOLECULAR DESIGN

Scheme 1. Design and Synthetic Scheme for Isoreticular MOF Series MPc-Cu-X (M=Co, Ni, X=NH, O) containing CoPc and NiPc units connected by Cu bis(diimine) and Cu bis(dioxolene) linkages.

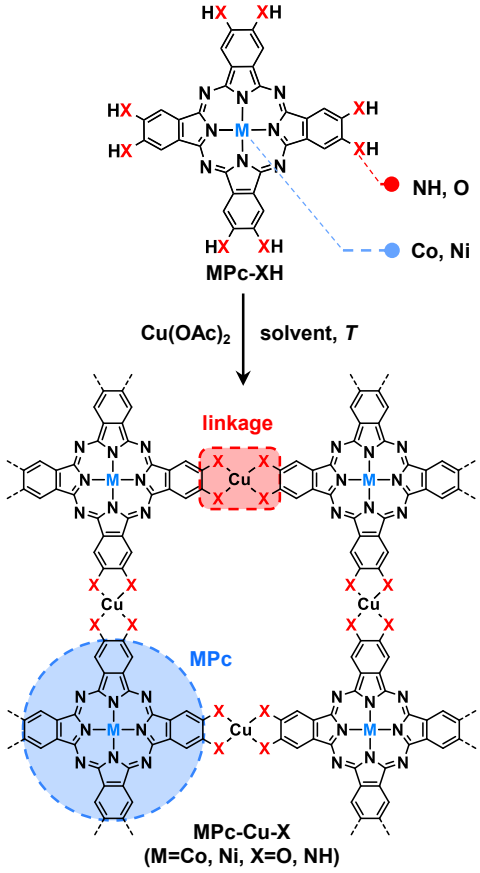

Our molecular design relies on the reticular incorporation of molecular CO_2 reduction catalyst, metallophthalocyanine,

as a building block into conductive, porous, and extended framework architectures. Four MPc-based ligands (2,3,9,10,16,17,23,24-octa-substituted metallophthalocyanine, general name, **MPc-XH**, see **Scheme 1**) were deliberately chosen to be integrated into conductive MOFs, which are CoPc and NiPc, respectively, bearing two types of heteroatoms (NH and O): **CoPc-NH$_2$**, **CoPc-OH**, **NiPc-NH$_2$**, and **NiPc-OH** We chose these particular MPc-based building blocks for three main reasons. *Firstly*, MPcs are known molecular catalysts for CO_2 reduction whose selectivity and activity highly depend on the identity of their metal cavities.[37, 73-74] Therefore, we employed two different types of MPcs, CoPc and NiPc, to realize a primary level tuning of catalytic performance. To confirm the critical role of the central metal within phthalocyanine in the catalytic CO_2 reduction we also used metal-free phthalocyanine-based analogs for comparison. *Secondly*, the peripheral functional groups with different heteroatoms decorating the outer rim of MPcs provide a secondary level of direct modifications of the electronic property of MPcs though their electronic communication within the large conjugated skeleton. This "*through-bond*" electronic modification at proximal positions of molecular catalysts with planar conjugated structures can be more effective than the "*through-space*" electronic effects, where the modifications are remote from the catalytic core.[58, 73, 75] *Thirdly*, the ortho-positioned amino and hydroxyl groups on tetratopic **MPc-XH** scaffolds, when coordinated to a variety of late transition-metal nodes, are capable of providing square-planar coordination geometry allowing the formation of 2D d-π conjugated structures, which are beneficial for the generation of materials with high intrinsic conductivity, [67-68, 76-77] which can promote high electrocatalytic activity.

All four MOFs in this study employed Cu ions as coordination nodes. Cu-based complexes previously have shown limited catalytic CO_2 to CO reduction capabilities,[57, 78-80] we anticipated a minimal contribution of the Cu-based nodes towards to target catalytic process. A potentially advantageous feature of this choice of the node is that the redox-active nature of Cu may result in a mixed valency state in the frameworks that can promote charge hopping and lead to enhanced conductivity in the general class of materials.[72]

We reasoned that the interconnection of **MPc-NH$_2$** and **MPc-OH** building blocks by the Cu nodes can provide access to an isoreticular series of bimetallic MPc-based MOFs **MPc-Cu-X** with four members: **CoPc-Cu-NH**, **CoPc-Cu-O**, **NiPc-Cu-NH**, and **NiPc-Cu-O**. **NiPc-Cu-O**, previously reported by us, was found to possess good conductivity and excellent chemiresistive gas sensing performance.[77] However, **NiPc-Cu-O**, together with the other three new MOFs featured in this work, has not been examined in the context of CO_2 reduction. Based on the above design considerations, we hypothesized that this design focusing on ligand-engineering will allow us to achieve an effective, hierarchical, and multifaceted tuning of the CO_2 to CO reduction performance, and make it possible to systematically study structure–property relationships of this class of materials in the context of their catalytic performance through the utilization of conductive frameworks materials. To confirm the critical role of the metal within the MPc unit on the catalytic performance of MOFs, and decouple the influence of this metal from that of Cu nodes, we employed two additional metal-free phthalocyanine-based MOFs **Pc-Cu-X**. Additionally, to establish the contribution of the framework structure over the **MPc-XH** monomer, the catalytic performance on the monomer units was also studied.

RESULTS AND DISCUSSION

Synthesis and Characterization of MOFs. Solvothermal conditions were used to integrate NiPc- and CoPc-based units into MOF structures through the self-assembly of the corresponding amino-and hydroxy-substituted MPc ligands with Cu(II) ions (**Scheme 1**, see **Section 2.7** in SI for synthetic details). Briefly, **CoPc-Cu-NH** and **CoPc-Cu-O** were prepared by reacting 2,3,9,10,16,17,23,24-octa-aminophthalocyanine cobalt(II) and 2,3,9,10,16,17,23,24-octa-hydroxylphthalocyanine cobalt(II) with copper acetate in a solvent mixture of dimethyl sulfoxide/water (3:1, v/v) under 65 °C and 85 °C, respectively. **NiPc-Cu-NH** and **NiPc-Cu-O** were made by the reaction between Cu(II) with 2,3,9,10,16,17,23,24-octa-aminophthalocyanine nickel(II), 2,3,9,10,16,17,23,24-octa-hydroxylphthalocyanine nickel(II), at 65 °C and 85 °C respectively in dimethyl sulfoxide. Similar to **MPc-Cu-X** MOFs, the metal-free phthalocyanine-based MOFs **Pc-Cu-O** and **Pc-Cu-NH** were synthesized by interconnecting the ligands phthalocyanine-2,3,9,10,16,17,23,24-octaol (**Pc-OH**) and phthalocyanine-2,3,9,10,16,17,23,24-octaamine (**Pc-NH$_2$**) with Cu nodes (**Scheme S8**, see also **Section 2.7** in SI for synthetic details).

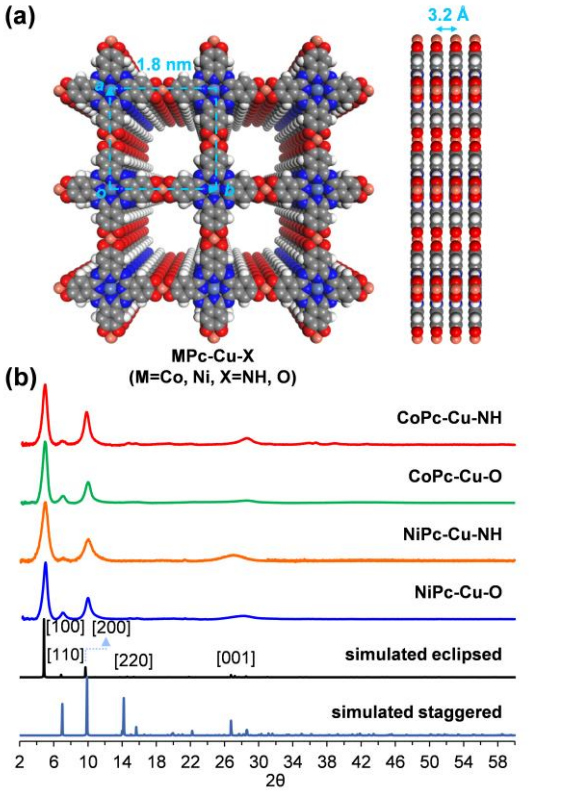

Figure 1. Structure and characterization of **MPc-Cu-X** MOFs. (a) Top and side view of a general structural representation of **MPc-Cu-X** MOFs with 2 × 2 square grids in eclipsed stacking mode. (b) Comparison of the experimental pXRD of MOFs with simulated pXRD with eclipsed and staggered packing mode.

The formation of the four MPc-containing crystalline MOFs (**Figure 1a**) was confirmed by powder X-ray

diffraction (pXRD). All four MOFs showed similar diffraction patterns with strong peaks at 2θ = 5.0°, 7.2°, 10.0°, and 28.0-28.5° (**Figure 1b**), assigned to [100], [110], [200], and [001] facets, respectively, consistent with their isoreticular structures. The strong diffractions from the [100], [110], [200] facets indicated good long-range order within the *ab* plane. The side length of the square lattice formed by the linkage between CoPc/NiPc and Cu nodes, based on those three diffractions, was calculated to be 1.8 nm. Compared with diffractions from facets orthogonal to the *ab* plane, the diffraction from [001] facet, which is parallel to the *ab* plane, is broader, indicating a diminished out-of-plane order. The [001] diffractions at 2θ=28.0–28.5° suggested a structural ordering with ~3.2 Å separations of layers along the *c* axis. Simulations using the model of *P4/mmm* space group with eclipsed cofacial AA-stacking, where MPc subunits were cofacially stacked in adjacent layers (**Figure 1a**), were consistent with the experimental results. The model of staggered packing of layers with an offset by $a/2$ and $b/2$ did not match the experimental pXRD pattern (**Figure 1b**). The formation of the MOFs was further confirmed by attenuated total reflectance Fourier transform infrared spectroscopy (FTIR) [81-84] (**Figures S9-S12**) and elemental analysis (**Section 5** in **SI**). These results are in good agreement with our earlier results[77] and other related MPc-based MOF system.[63, 82] pXRD (**Figures S33**, **S34**) and FTIR (**Figures S13**, **S14**) characterizations also suggested desired square network structures for **Pc-Cu-X** MOFs, resembling **MPc-Cu-X** MOFs (**Figure S27**). Although investigation based on triphenylene-based conductive MOFs has revealed that differences in the crystal system can contribute to differences in electrochemical O_2 reduction,[85] we believe that the isostructural **MPc-Cu-X** and **Pc-Cu-X** MOFs with square lattices presented in this study is beneficial for a systematic investigation of discrete structural features within these materials, thus enabling the comparison of their catalytic activity in electrochemical CO_2 reduction.

Scanning electron microscopy (SEM) revealed nanoscale morphology in all the four MOFs (**Figures 2a-2d**). **CoPc-Cu-NH** exhibited a distribution of irregularly shaped crystallites with dimensions of a few tens of nanometers (**Figure 2a, Figure S45b**). Both **CoPc-Cu-O** and **NiPc-Cu-NH** showed sub-micrometer-sized aggregates consisting of non-uniform rods or grains (**Figures 2b, 2c, Figures S47b, S49b**). **NiPc-Cu-O** exhibited flake-like morphology, which coexisted with sub-micrometer sized grains **(Figure 2d, Figure S51b)**. **Pc-Cu-NH** and **Pc-Cu-O** both showed sub-micrometer-sized aggregates (**Figures S53, S54**). High-resolution transmission electron microscopy (HR-TEM) provided direct visualization of square pores with a side length of ~1.8 nm for **CoPc-Cu-NH, NiPc-Cu-NH,** and **NiPc-Cu-O** (**Figures 2e, 2g, 2h**), which is in good agreement with the values calculated from pXRD ([100], [200] peak). Parallel lines with characteristic spacings of ~1.8 nm were also observed for **CoPc-Cu-O** (**Figure 2f**). Energy-dispersive X-ray spectroscopy mapping of the M**Pc-Cu-X** and **Pc-Cu-X** MOFs all revealed a homogeneous distribution of the C, N, and/or O, as well as the metal elements, including Cu or Co or Ni through the sample region on the micrometer scale (**Figures S45, S47, S49, S51, S53, S54**).

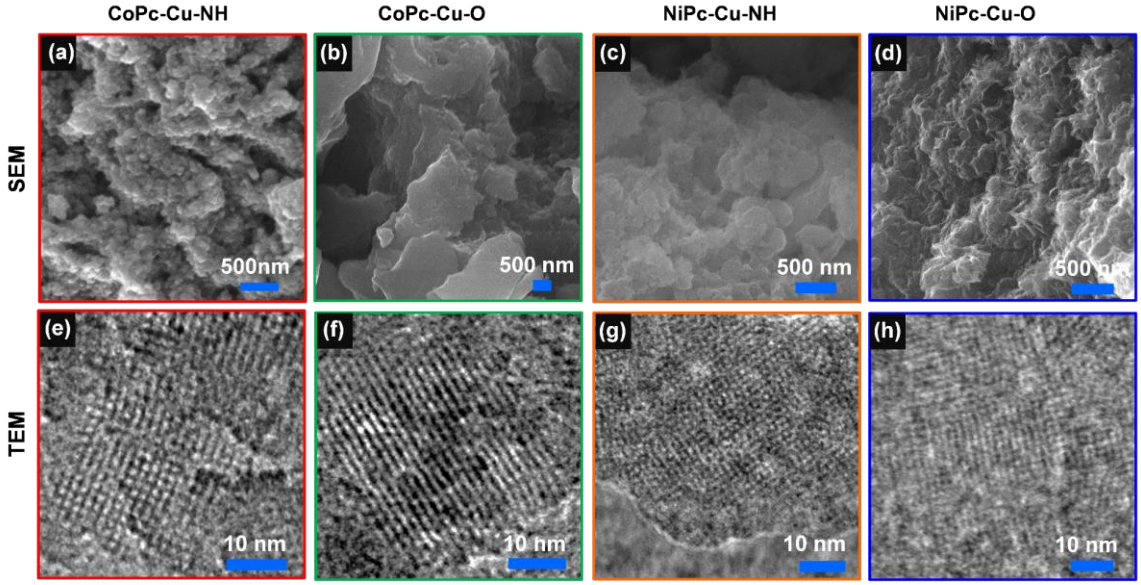

Figure 2. (a)-(d) SEM images and (e)-(h) TEM images for **CoPc-Cu-NH**, **CoPc-Cu-O**, **NiPc-Cu-NH**, and **NiPc-Cu-O** MOFs.

High-resolution X-ray photoelectron spectroscopy (XPS) showed that in all these **MPc-Cu-X** and **Pc-Cu-X** MOFs, the Cu $2p_{3/2}$ range could be clearly deconvoluted into two peaks at the binding energies of 932.9 and 935.0 eV, indicating that Cu nodes existed as a mixed state of Cu(I) and Cu(II)[86-87] (**Figures S16c, S18d, S20c, S22d, S24b, S26c**). The observations of mixed valency of Cu were also consistent with other Cu containing d-π conjugated MOFs.[72, 88] XPS data also suggested that Co and Ni in the **MPc-Cu-X** MOFs presented as Co^{2+} and Ni^{2+}, respectively (**Figures S16b, S18c, S20b, S22c**). The presence of the paramagnetic Cu(II) and/or Co(II) was also consistent with the electron paramagnetic resonance spectra, where metal central radicals were observed (**Figures S39-S44**).

The electrical conductivity of the **MPc-Cu-X** and **Pc-Cu-X** MOFs was measured at room temperature on the pressed pellets using a four-point probe method (see **Section 12** in Supporting Information). The conductivities were 5.79 × 10^{-}

^{2}, 2.12 × 10^{-2}, 2.73 × 10^{-3}, and 1.04 × 10^{-1} S cm^{-1} for **CoPc-Cu-NH**, **CoPc-Cu-O**, **NiPc-Cu-NH**, and **NiPc-Cu-O**, respectively. Compared with other MPc-based MOFs made from octasubstituted MPcs, these conductivities values are comparable with NiPc-MOF,[82] and Fe_2[PcFe–O_8],[89] and higher than Cu-CuPc[90] and MOF-1992•[Fe]$_3$.[59] The conductivity of **NiPc-Cu-O** is about 7 times higher than our previous report (featured as NiPc-Cu),[77] which is probably due to the partial oxidation of the material considering its p-type semiconductive feature (see **section 12** in Supporting Information**)**. The conductivity values of these MOFs were in a similar range with metal-bis(dioxolene)-linked MOFs and metal-bis(diimine)-linked MOFs.[67, 76, 91-95] DFT calculations by using the CASTEP module in Materials Studio 2019 with Perdew–Burke–Ernzerhof generalized gradient approximation revealed dispersed electronic band structures that cross the Fermi level for all MOFs (**Figures S36**, **S37**), which are consistent with their good conductivities.[91, 96-98] Importantly, compared with the molecular CoPc and NiPc analogs, which usually have conductivities in the range of 10^{-10}-10^{-12} S cm^{-1},[99-101] embedding NiPc and CoPc subunits into framework structures improved the conductivity by more than 7 orders of magnitude. The conductivities of the comparison MOFs **Pc-Cu-NH** and **Pc-Cu-O** were 3.72 × 10^{-5} and 5.32 × 10^{-3} S cm^{-1}, respectively. We believe that the good electrical conductivities of these MOFs are beneficial for the charge transport during the electrochemical reduction of CO_2, and therefore, can contribute to improved current densities.

To assess the porosity and specific surface area of the MOFs, N_2 gas sorption isotherms at 77 K were performed. The Brunauer–Emmett–Teller surface areas for **CoPc-Cu-NH**, **CoPc-Cu-O**, **NiPc-Cu-NH**, **NiPc-Cu-O, Pc-Cu-NH,** and **Pc-Cu-O** were 349, 582, 628, 421, 181, 364 m^2 g^{-1}, respectively. (**Figures S55-S60**). Encouraged by the large surface area of these MOFs, we further tested their CO_2 adsorption ability at 298 K. The CO_2 uptake is paramount to CO_2 conversion, because CO_2 adsorption can increase the local concentration of CO_2 around the catalytically active sites of materials even at low CO_2 concentrations in the bulk electrolyte solution. The pre-absorbed CO_2 may potentially be activated by the functional group presented in the materials, further improving catalytic efficiencies of MOFs.[4, 74, 102-105] As shown in **Figure S61**, the CO_2 uptake at room temperature by **CoPc-Cu-NH**, **CoPc-Cu-O**, **NiPc-Cu-NH**, **NiPc-Cu-O, Pc-Cu-NH,** and **Pc-Cu-O** reached 1.48, 2.03, 1.90, 1.56, 0.57, 1.02 mmol g^{-1} under a CO_2 pressure of 900 Torr.

Heteroatomic Crosslinker-Dependent Redox activity of MPc-Cu-X MOFs. To study the electrochemical properties of the MPc MOFs, a slurry containing MOFs and CB (a mass ratio of 1.0:0.5) and Nafion (2.5%) in water was prepared and drop-casted on the carbon fiber electrodes (see **Section 13.1** in Supporting Information for details). As suggested by precedent,[56, 59-60] creating a composite of MOFs with CB can enhance the conductivity of the active material and the use of Nafion can promote the formation of a homogeneous dispersions of MOFs. In this study, we initially adopted a 1.0:0.5 mass ratio of MOF/CB to minimize the use of the conductive matrix, while ensuring sufficient conductivity. The electrochemical characterization of the MOF/CB cathode was performed in a three-electrode cell with a Pt mesh as the counter electrode and saturated calomel electrode as the reference electrode in a 0.2 M aqueous solution of $KHCO_3$.

All the four **MPc-Cu-X** MOFs did not exhibit noticeable redox activity in a nitrogen-saturated solution at the potential window of 0.16-1.36 V (vs reversible hydrogen electrode, RHE) with a scan rate of 10 mV s^{-1} (dash traces in **Figures 3a-d**), but showed pronounced redox activity in a CO_2-saturated $KHCO_3$ solution (pH=6.8) that correlated with the identity of the heteroatomic crosslinker. **CoPc-Cu-NH** and **NiPc-Cu-NH** MOFs with NH linkers (solid traces in **Figures 3a, 3c**) at a scan rate of 10 mV s^{-1} showed an anodic peak centered at 0.67−0.69 V (vs RHE) and a weak cathodic peak centered around 0.50−0.53 V (vs RHE), respectively. Under the same conditions, the CV curves of **CoPc-Cu-O** and **NiPc-Cu-O** showed strong anodic peaks at 0.76−0.77 V (vs RHE) and broad cathodic peaks around 0.48 V (vs RHE, **Figure 3b, 3d**). The charge quantity

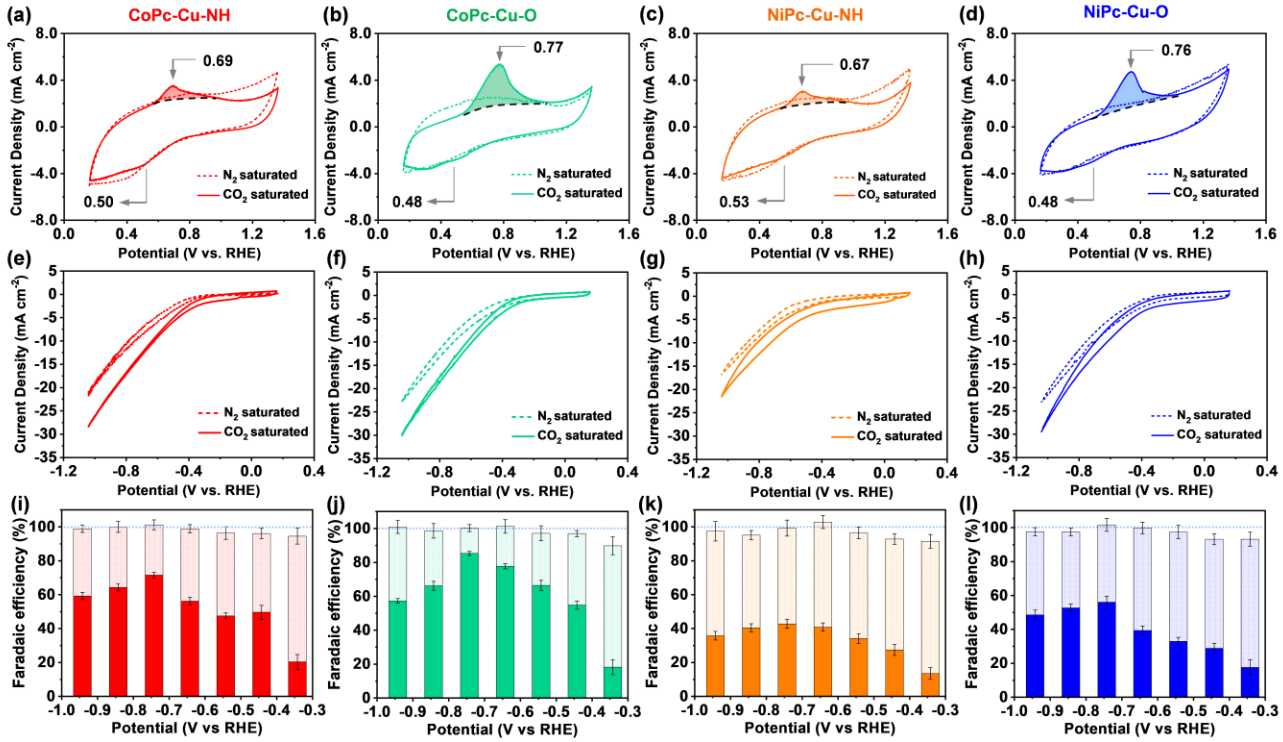

Figure 3. (a)-(d) Cyclic voltammetry (CV) for MOFs/CB (mass ratio=1.0:0.5) at potential range of 0.16-1.36 V (vs RHE, scan rate: 10 mV s^{-1}) in a CO_2-saturated (solid line, pH=6.8,) and N_2-saturated (dashed line, pH=7.2) $KHCO_3$ solution. **(e)-(f)** CV for MOFs at the potential range of –1.04-0.16 V (vs RHE, scan rate: 10 mV s^{-1}). **(i)-(l)** Faradaic efficiencies for the products from the catalytic reduction at different potentials (solid-filled columns for CO and pattern-filled columns for H_2).

corresponding to the oxidation peak for **CoPc-Cu-O** and **NiPc-Cu-O** were 91.2 and 51.84 mC, respectively, which were larger than their analogs with NH heteroatomic linkers (37.7 and 35.1 mC for **CoPc-Cu-NH** and **NiPc-Cu-NH**, respectively, **Figure S71**). These values indicated that the number of electroactive sites of **MPc-Cu-O** MOFs cathode was higher than the corresponding **MPc-Cu-NH** counterparts.[59]

Considering the dependency of the anodic peak positions on the heteroatoms of the MPc ligands and the observed consistency of the anodic peak positions of these MOFs with that of the reported MOF containing CoPc catecholate units measured at similar conditions,[59] we ascribed the anodic peaks observed at the scan rate of 10 mV s^{-1} to the $4e^-$ oxidation from CoPc/NiPc catecholate to CoPc/NiPc semiquinolate (**Scheme S9**, see **section S13.2** in Supporting Information for discussion). The weak cathodic peaks centered around 0.50–0.53 V (vs RHE) gradually disappeared with the increase of the scan rate (**Figure S70**), indicating irreversible processes that might be associated with the reduction of the CoPc/NiPc semiquinolate units. The estimated electroactive coverage for **CoPc-Cu-NH**, **CoPc-Cu-O**, **NiPc-Cu-NH**, and **NiPc-Cu-O** based on the charge quantity of the anodic peaks were 37.7, 91.2, 35.1, and 51.8 nmol cm^{-2}, respectively. These observed differences in position and intensity of anodic peaks between MOFs with NH and O heteroatomic linkers strongly suggested that the heteroatom substituents on MPc core have an appreciable effect on their redox activity, which were expected to further influence their catalytic behavior for CO_2 reduction.

Electrocatalytic Performance of MOFs in CO_2 Reduction. To estimate the electrochemical CO_2 reduction performance of the four MOFs and study the structure–property relationship, we started the test by using their composite with CB with the same mass ratio of 1.0:0.5 under the same conditions (section **S13.2 in Supporting Information**). With the applied cathodic potentials, all of the four MOFs in the N_2-saturated $KHCO_3$ electrolyte showed an exponential increase of current density that was ascribed to the H^+ reduction ($2H^+ + 2e^- \rightarrow H_2$) (**Figures 3e-3h**). In the CO_2-saturated $KHCO_3$ electrolyte, enhanced current intensities were observed. The current density under the CO_2-saturated atmosphere was associated with the catalytic CO_2 reduction ($CO_2 + 2H^+ + 2e^- \rightarrow CO + H_2O$) and/or H^+ reduction. Since the current density is a function of the kinetics of various electron transfer processes between the substrate and the electrode material,[48-49] the increased current densities obtained in CO_2-saturated electrolyte compared with that in N_2-saturated electrolyte indicated the significant contribution of the current due to the CO_2 reduction process.

To assess the energy efficiency and selectivity of the MOFs for CO_2 reduction, electrolysis was performed at various fixed potentials ranging from −0.34 to −0.94 V (vs RHE) for 2400 s. Gas chromatography was used to determine the identity and quantity of the gaseous products. As illustrated in **Figures 3i-3l**, two gaseous products, CO and H_2, dominated the distribution of the products within the tested potentials. Even at a low voltage of −0.44 V vs RHE, corresponding to a small overpotential of −0.33 V, the faradaic efficiency for CO reached significant values of 50%, 55%, 27%, and 29% for **CoPc-Cu-NH**, **CoPc-Cu-O**, **NiPc-Cu-NH**, and **NiPc-Cu-O**, receptively (**Figures 3i-3l**). The small

overpotential demonstrated excellent energy efficiency of the electrochemical transformation. In the electrolysis potential range from −0.44 to −0.74 V (vs RHE), FE_{co} showed an increasing trend when more negative potentials were applied. At the potential of −0.74 V (η=−0.63 V), FE_{co} values reached their maximum. **CoPc-Cu-NH**, **CoPc-Cu-O**, **NiPc-Cu-NH**, and **NiPc-Cu-O** achieved FE_{co} of 72%, 85%, 43%, and 56%, respectively. The average steady-state current density at the potential of −0.74 V reached −11.6, −13.2, −6.1, and −7.3 mA cm^{-2}, respectively. These sustained current densities achieved in this study are about 5.1–10.9 times of that obtained for MOF-545Fe/CB,[56] 6.1–13.1 times of that obtained for $Al_2(OH)_2$TCPP-Co,[49] 1.8–4.0 times of that obtained by COF-367-Co,[61] 1.5-3.3 times of that obtained by PcCu-O_8-Zn,[63] 0.37-0.79 times of that obtained by MOF-1992/CB, and 0.27-0.59 times of that obtained by CoPc-PDQ-COF[65] at similar overpotentials (see **Table S11**).[59] At reducing electrode potentials exceeding −0.74 V, the Faradaic efficiencies for CO production tended to decrease, while H_2 evolution increased. Liquid products, including formic acid, methanol, and acetic acid, were also found at the potential of −0.74 V (vs RHE) but with very small fractions (<<5%, see **section 13.4** in Supporting Information).

Compared with the corresponding **MPc-XH** ligands, **CoPc-Cu-NH**, **CoPc-Cu-O**, and **NiPc-Cu-O** MOFs showed higher selectivity for the production of CO at the tested potential ranges; the FE_{CO} obtained by **NiPc-Cu-NH** and **NiPc-NH_2** were comparable (**Figures S82-S83**). All these MOFs achieved significantly higher current densities at most of the tested potential ranges. At the potential of −0.74 V (vs RHE), the current densities obtained by **CoPc-Cu-NH**, **CoPc-Cu-O**, **NiPc-Cu-NH**, and **NiPc-Cu-O** were 20%, 36%, 26%, and 35% higher than those obtained by the corresponding ligands, respectively (**Figure S83**).

A close observation of the FE_{co} at different potentials for the four MOFs revealed two important structure-dependent features. *First*, under all the tested potentials CoPc-based MOFs exhibited higher activity (higher *j* values) and selectivity (higher FE_{co} values) toward CO product than NiPc–based analogs. This feature was particularly prominent for most of the potentials in the range of −0.44 to −0.94 V (vs RHE). *Second*, the MOFs with O crosslinkers were superior in activity and selectivity than the corresponding NH-linked analogs. The observation that CoPc–containing MOFs showed higher performance than the NiPc containing counterparts indicated that the nature of the catalytic active sites has an impact on the CO_2 reduction performance of reticular materials. This observation is consistent with the previous investigation on molecular MPc–based catalysts in which CoPc exhibited the optimum activity compared with MnPc, FePc, NiPc, and CuPc.[79] The influence of the heteroatom around the catalytic active MPc sites suggested that CO_2 reduction performance of MOFs can be further tuned through the modulation of the electronic environment around the active site by different types of substituent.[58, 73] This approach is consistent with the precedent where substituents with different electron-donating or electron-withdrawing features on the catalytic centers can facilitate the formation of key intermediates and/or promote the CO desorption to boost the catalytic conversion.[37, 73, 75, 106]

Although the metal cavity of MPcs and the heteroatomic linkages can both influence the CO_2 reduction performance, the contributions of these two factors are not equivalent. For the seven tested potentials from −0.44 to −0.94 V (vs RHE), the average FE_{co} difference (ΔFE_{co}) due to the difference of metal center of MPcs was 19% and 21% for MOFs with NH and O crosslinkers, respectively; while the average ΔFE_{co} resulted from crosslinker difference was only 8% and 6% for CoPc- and NiPc-based MOFs, respectively. Similarly, the average current density difference (Δj) resulting from the different metal inside MPcs was 4.3 and 4.1 mA cm^{-2} for MOFs with NH and O crosslinkers, respectively. These values are much larger than Δj resulting from crosslinker difference, which was only 0.4 and 0.7 mA cm^{-2} for CoPc- and NiPc-based MOFs, respectively. These comparisons suggested that a dual-level modulation was indeed realized by the choice of a combination of the metal cavity of MPcs and the heteroatomic linkages.

When plotting the partial current density for CO production on a logarithmic scale versus thermodynamic overpotential at low overpotential ranges (**Figure S79**), Tafel slopes of 165, 171, 351, and 327 mV $decade^{-1}$ were obtained for **CoPc-Cu-NH**, **CoPc-Cu-O**, **NiPc-Cu-NH**, and **NiPc-Cu-O**, respectively. The values of Tafel slopes indicated that the formation of CO catalyzed by CoPc-based MOFs was more kinetically favorable than that by NiPc MOFs.[107-110] The electrochemical impedance spectroscopy (EIS) was performed at a bias voltage of −0.74 V (vs RHE) to measure the charge transfer resistance (R_{ct}) of the four MOFs, which can be correlated to the impedance of electrons transfer between the catalyst surface and the reactant, as well as intermediate formation inside the double layer.[23] EIS experimental results (**Figure S80**) showed that R_{ct} values for **CoPc-Cu-NH** and **CoPc-Cu-O** are 5.6 and 2.4 Ohms, respectively, versus 8.8 ohms for **NiPc-Cu-NH** and 6.5 Ohms for **NiPc-Cu-O**, which suggested the faster electron transfer between CoPc-based MOFs and reaction species than those for NiPc-based MOFs.

To examine the stability and durability of the MOFs, the electrolysis was further tested over an extended period of time under a fixed potential of −0.74 V (vs RHE) in CO_2-saturated aqueous $KHCO_3$ solution. All four MOFs showed stable current densities without significant decay over a 10 h period (**Figure 4a**). pXRD of the four **MPc-Cu-X** MOFs after electrolysis showed that they still maintained their crystalline framework structure (**Figure S91**). Meanwhile, no obvious morphology change of the electrode materials could be observed after test (**Figure S92**). All these results indicated excellent stability of these materials during the electrochemical catalysis process. During this period, the average FE_{CO} was 72%, 84%, 43%, and 58% for **CoPc-Cu-NH**, **CoPc-Cu-O**, **NiPc-Cu-NH**, and **NiPc-Cu-O**, respectively. For **CoPc-Cu-O**, about 2.09 mmol of CO accumulated during the 10 h period, which corresponded to a total turnover number of 22,681 and a turnover frequency (TOF) of 0.63 s^{-1} for the conversion of CO_2 to CO (**Table S10**). This TOF value surpasses those obtained by other reported reticular materials.[49, 56, 59-61, 63-64, 111]

Although reticular materials have recently emerged as a new generation of catalysts for electrochemical reduction of CO_2 to CO, recognized for the feasibility of atomically precise arrangement of molecular catalysts, open and porous

architecture, and the potential for modular control of chemical and structural features to rectify the activity, selectivity, and efficiency, they have not yet been employed as electrocatalysts in pure form, without the addition of conductive binders.[4, 48] The previously reported systems based on reticular material relied heavily on the use of the external conductive matrix, including acetylene black, CB, or carbon nanotube (CNT), to form composite electrode materials, because the poor to moderate electrical conductivity in these reticular materials is a major constraint for them being used as efficient electrocatalysts.[49, 56-61, 63-64] Encouraged by the good electrical conductivity of **CoPc-Cu-O** and the most promising catalytic performance obtained from the composite of **CoPc-Cu-O/CB** (mass ratio=1:0.5) as demonstrated in **Figure 3**, we further sought to test the performance of **CoPc-Cu-O** as a standalone catalyst, in conjunction with composites made of **CoPc-Cu-O** and carbon black with other mass ratios.

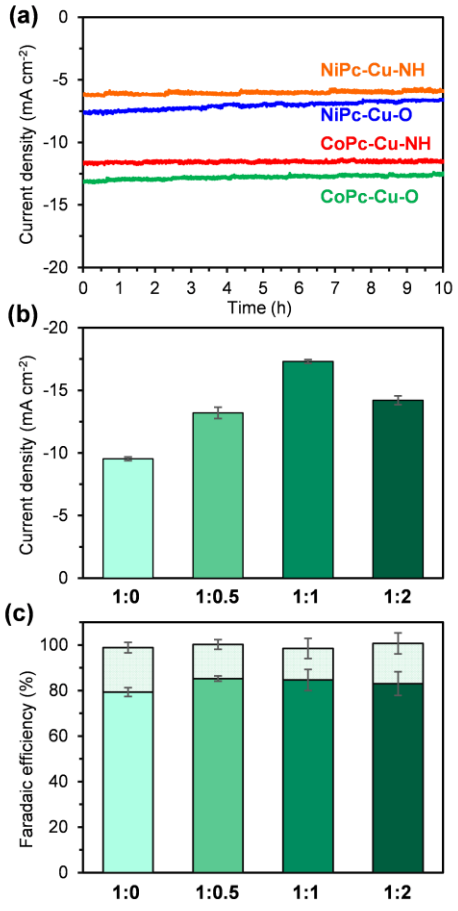

Figure 4. (a) Chronoamperometry for 10 hours at a fixed potential of −0.74 V vs (RHE) for the four MOFs in a CO_2-saturated $KHCO_3$ solution (pH=6.8). Comparison of **(b)** current densities at a fixed potential of −0.74 V vs (RHE) and **(c)** FE for electrodes made of **CoPc-Cu-O** and carbon black with mass ratios of 1:0, 1:0.5, 1:1, and 1:2 (solid-filled columns for CO and pattern-filled columns for H_2).

Under the fixed potential of −0.74 V (vs RHE) in CO_2-saturated aqueous $KHCO_3$ solution, the composite of **CoPc-Cu-O** and CB in ratio of 1:1 and 1:2, respectively, gave high current densities of −17.3 and −14.1 mA cm^{-2} with FE_{CO} values of 85% and 83% (**Figures 4b, 4c, Figure S85**). Moreover, when **CoPc-Cu-O** was used as the sole active material without any conductive additives, a current density of −9.5 mA cm^{-2} was achieved with a FE_{CO} of 79% (**Figures 4b, 4c, Figure S84**). Balancing both the current density and FE values, **CoPc-Cu-O** gave the best performance than other systems that apply reticular frameworks as the only active materials (see also **Table S11**).[49, 61-62, 64, 111-112]

Mechanistic Study. To investigate the catalytic mechanism and the underlying structure–performance relationship of the four MOFs, we performed a series of comparison experiments and DFT calculations.

Comparison experiments. **MPc-Cu-X** MOFs contain two types of the metal-centered cites, the Co/Ni centers of the MPc and the Cu centers embedded in bis(diimine) or bis(dioxolene) units, both of which can theoretically play a role in CO_2 reduction. Since Cu-based complexes usually exhibit limited catalytic CO_2 to CO reduction capabilities,[57, 78-80] we hypothesized that MPc centers were key catalytic sites in the **MPc-Cu-X** MOFs. To test this hypothesis, we tested **Pc-Cu-NH** and **Pc-Cu-O** for comparison (**section S13.3** in Supporting Information). In these **Pc-Cu-X** MOFs, **Pc-OH** and **Pc-NH_2** are interconnected by Cu with O and NH heteroatomic linkers to form meal-free Pc-based MOFs containing Cu bis(diimine) and Cu bis(dioxolene) units as the only possible active sites in their skeleton, respectively. The CO_2 reduction performance was tested using the same conditions that were used for the four **MPc-Cu-X** (M=Co, Ni; X=O, NH) MOFs. FE_{CO} values obtained at the potential range of −0.34 to −0.94 V (vs RHE) from **Pc-Cu-NH** and **Pc-Cu-O** were only 0.9-4.5% and 1.1-5.6%, respectively (**Figures S86, S87**). H_2 was found to be the dominant gaseous product. This important control experiment confirmed the critical role of the metal within the MPc subunit for promoting the catalytic reduction of CO_2 to CO.

We also conducted comparison experiments for CO_2 reduction test by employing two previously reported MOFs, $Cu_3(HITP)_2$ and $Cu_3(HHTP)_2$ (HITP = 2,3,6,7,10,11-hexaiminotriphenylene, HHTP = 2,3,6,7,10,11-hexahydroxytriphenylene) that contain only Cu bis(diimine) or Cu bis(dioxolene) fragments, respectively (**Figure S88**). Similarly, FE_{CO} values obtained from $Cu_3(HITP)_2$ and $Cu_3(HHTP)_2$ were 0.7-3.3% and 0.9-4.3% respectively, at the potential range of −0.34 to −0.94 V (vs RHE). The averaged FE values for H_2 were 92% and 83% for $Cu_3(HITP)_2$ and $Cu_3(HHTP)_2$, respectively.

Taken together, the results of these two control experiments supported our hypothesis that Cu bis(diimine) and Cu bis(dioxolene) centers within the four comparison MOFs were inert in catalyzing the electrochemical reduction of CO_2 to CO under the tested conditions. These observations are consistent with other copper-based coordination complexes or MOFs which usually showed very limited catalytic activity in the electrochemical conversion of CO_2 to CO under similar electrolysis conditions, for example, CuPc (FE_{CO}<10%),[57, 78-79] [Cu(cyclam)]Cl_2 (FE_{CO}<1%),[78] and Cu(BTC) (FE_{CO}<5%).[78, 80] These prior reports, combined with our control experiments, further reinforce that the catalytic performance of **MPc-Cu-X** MOFs in the electrochemical reduction of CO_2 to CO is likely dominated by the MPc units.

Computational study. The electrochemical reduction of CO_2 to CO at the cathode is a two-proton-electron (2 H^+/e^-) transfer process.[7, 31, 113] In the first proton-electron transfer process which may happen in a concerted[31, 114] or a sequential manner, a carboxyl intermediate [**P**-COOH] (**P** indicates the active site of the catalyst) is

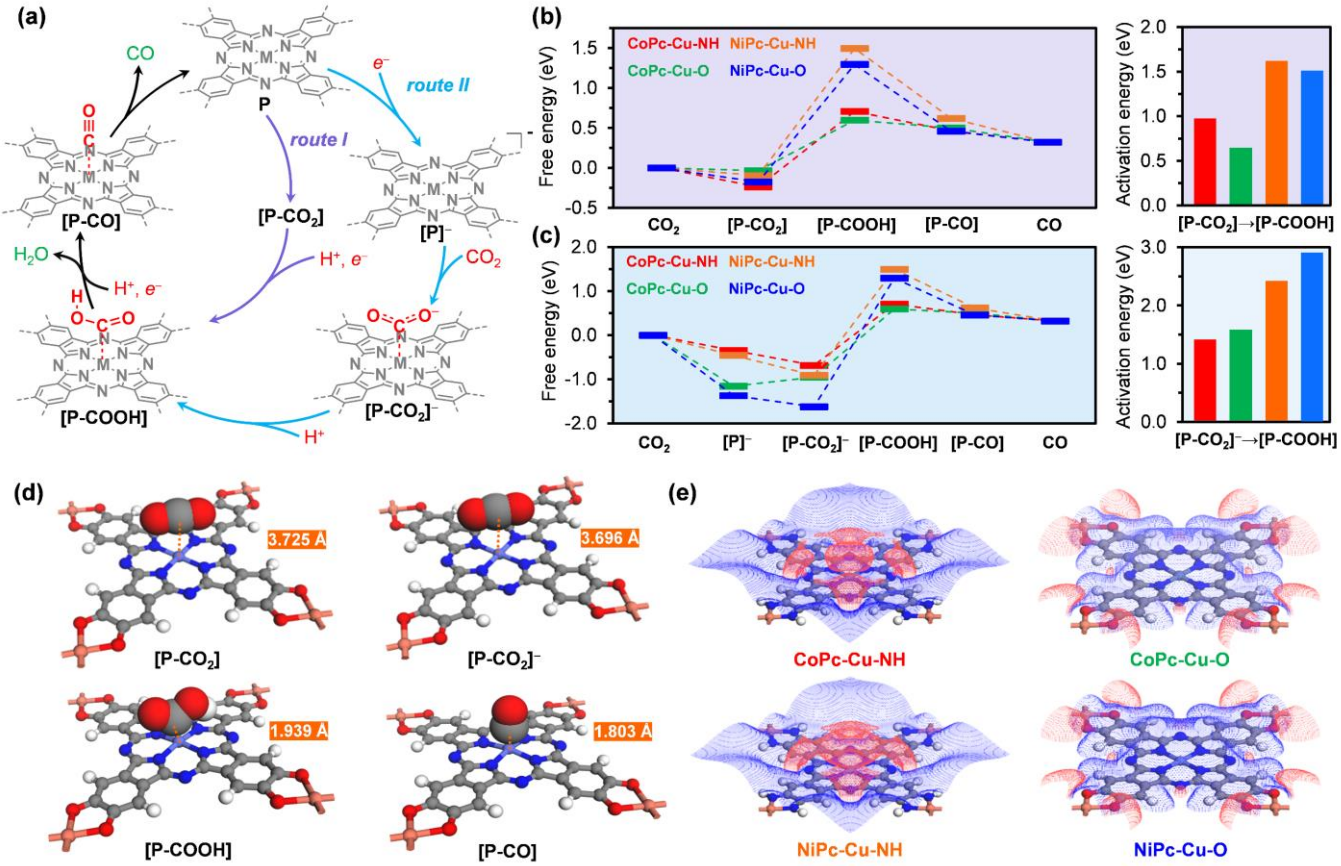

Figure 5. (a) Proposed catalytic mechanism for electrochemical reduction of CO_2 to CO by MPc sites of **MPc-Cu-XH** MOFs which contains two reaction pathways: *route I* and *route II*. Free energy profiles for electrochemical reduction of CO_2 to CO catalyzed by **CoPc-Cu-NH** (red), **CoPc-Cu-O** (green), **NiPc-Cu-NH** (orange), and **NiPc-Cu-O** (blue) under *the* standard condition and electrode potential of 0 V (vs standard hydrogen electrode) through the reaction pathway of (b) *route I* and (c) *route II.* In *route I* and *route II*, the steps with the highest activation energy values are [**P**-CO_2]→[**P**-COOH] and [**P**-CO_2]$^-$→[**P**-COOH], respectively. The activation energy values are plotted on the right side as bar graphs and color-coded for the four MOFs correspondingly. (d) Structures of the catalyst and key reaction intermediates involved in the proposed reaction mechanism for **CoPc-Cu-O** mediated reaction. (e) Electrostatic potential maps of the **MPc-Cu-XH** MOFs with isovalue set at 0.5 eV.

formed.[115-117] Then, a second H^+/e^- can subsequently attack the oxygen atom of the OH group in [**P**-COOH] to form H_2O and [**P**-CO]. The active site-bounded carbon monoxide [**P**-CO] finally desorbs from the electrode to generate free CO. So, the electrochemical reduction of CO_2 to CO generally contains four elementary reactions, which include the CO_2 adsorption, the formation of [**P**-COOH], the formation of [**P**-CO], and the final CO desorption step.[31, 60] As the first proton-electron transfer may happen in a sequential manner, we proposed two possible reaction pathways, *route I* and *route II* as shown in **Figure 5a,** to reveal the underlying reaction mechanism. The difference between *route I* and *route II* is that the formation of [**P**-COOH] in the former is through a concerted H^+/e^- transfer to CO_2 absorbed species [**P**-CO_2], while in the latter the formation of [**P**-COOH] involves CO_2 adsorption on the one-electron reduced active site [**P**]$^-$ to form [**P**-CO_2]$^-$ before a subsequent proton transfer process.

To gain additional insight into the CO_2 to CO reduction process catalyzed by the MPc sites of MOFs, DFT calculations using generalized gradient approximation with Perdew-Becke-Ernzerhof as the exchange-correlation function were performed using Dmol^3 module in Materials Studio 2019 on the model of MOF monolayer to optimize the structures of the intermediates (**Figures S95-S98**) involved in the two proposed pathways and to calculate their free energies (See **Section S14** in Supporting Information for the details of the calculations). The calculated free energy (ΔG) diagram following *route I* showed that the rate-determining step in the CO_2 to CO conversion for the four MOFs is the formation of the [**P**-COOH] from the CO_2-absorbed species [**P**-CO_2] through the first H^+/e^- transfer process, which is likely due to the weak COOH binding at the MPc sites.[79, 118] The calculated energy barriers for the rate-determining steps were 0.95, 0.63, 1.59, and 1.47 eV for **CoPc-Cu-NH**, **CoPc-Cu-O**, **NiPc-Cu-NH**, and **NiPc-Cu-O** MOFs, respectively (**Figure 5b, Figure S99**). The lowered energy barrier found for CoPc-based MOFs compared with NiPc-based analogs were in good agreement with trends observed experimentally where CoPc-based MOFs gave higher CO current densities. The slightly lower energy barrier for the MOFs with O linkers compared with the NH linked analogs also suggested a heteroatom linker-based activity, which was

consistent with the experiment results. Computational results showed that COOH binding at MOFs with O linkers had relatively lower free energies than that with NH linkers ($\Delta\Delta G$=0.11 eV for CoPc-based MOFs, and $\Delta\Delta G$=0.20 eV for NiPc-based MOFs). DFT calculations on partial atomic charge and electrostatic potential of **MPc-Cu-X** MOFs both suggested a clear electronic effect resulting from the different types of linker: MOFs with O linkers have higher positive charges (**Figure S103**) and more positive electrostatic potential around the metal center of the MPc unit than MOFs with NH linkers (**Figure 5e, Figure S104**), suggesting that O-linked MOFs may stabilize the COOH intermediate to a better degree than their NH-linked analogs.

The calculated free energy diagram for *route II* revealed activation energies of 1.39-2.91 eV for the first the H^+/e^- transfer process that happened in a sequential manner (**Figure 5c, Figure S100**). These corresponding energies barriers in *route II* also indicated a MPc-based selectivity, similar to that in *route I*. However, they were 0.44-1.38 eV higher than those in *route I*, suggesting that the first H^+/e^- transfer process would be more likely to proceed in a concerted manner, rather in a sequential manner. In the optimized structure of the possible intermediates for **CoPc-Cu-O** catalyzed process (**Figure 5d**), the observed Co–CO_2 distance for [**P**-CO_2]$^-$ is shorter than that in [**P**-CO_2]. These results indicated that [**P**-CO_2]$^-$ species was a more energetically stable species than [**P**-CO_2], which will consequently lead to a higher energy barrier for the conversion of [**P**-CO_2]$^-$→[**P**-COOH] than that for [**P**-CO_2]→[**P**-COOH].

Examination of the CO_2 to CO process as being catalyzed by the Cu bis(dioxolene) or Cu bis(diimine) sites of MOFs gave the following energy barriers for the rate-determining step: 1.39, 1.22, 1.71, and 1.41 eV for **CoPc-Cu-NH**, **CoPc-Cu-O**, **NiPc-Cu-NH**, and **NiPc-Cu-O**, respectively (**Figure S105**). All these values, with the exception of **NiPc-Cu-O,** are larger than those for MPc site-catalyzed process, which reinforced our previous hypothesis that catalytic CO_2 to CO performance of these MOFs is likely dominated by the MPc units. The close activation energies ($\Delta\Delta G$=0.06 eV) for the case of **NiPc-Cu-O** suggested that Cu bis(dioxolene) site may also contribute to the generation of CO.

We further investigated the activity of the MOFs for hydrogen evolution process catalyzed by their MPc and Cu bis(dioxolene) or Cu bis(diimine) sites. The calculated results showed that hydrogen evolution process is more kinetically favorable at the MPc sites than at the Cu bis(dioxolene) or Cu bis(diimine) sites with energy barriers of 0.86, 0.82, 1.60, 1.24 eV for **CoPc-Cu-NH**, **CoPc-Cu-O**, **NiPc-Cu-NH**, and **NiPc-Cu-O**, respectively (**Figures S106-S107**). The magnitude of these values followed a very similar trend to those for the CO_2 reduction process: the values for CoPc-based and O-linked MOFs were respectively smaller than NiPc-based and NH-linked analogs. The results indicated that CoPc-based and O-linked MOFs likely enable faster H^+/e^- transfer kinetics than NiPc-based and NH-linked analogs. This feature may be beneficial for the formation of [**P**-COOH] and [**P**-CO] species by coupling [**P**-H] formed at one MPc site respectively with [**P**-CO_2] and [**P**-COOH] formed at the adjacent MPc site through H transfer process.[63]

CONCLUSION

We have developed for the first time an isoreticular series of the conductive MOFs that incorporate CoPc and NiPc with two types of heteroatoms (NH and O) by Cu nodes as catalysts for the electrochemical conversion of CO_2 to CO. Electrochemical test showed that the choice of a combination of the metal cavity in MPcs and the heteroatomic linkages in these materials achieved a dual-level reticular tuning of the catalytic efficiency CO_2 reduction performance, in which the activity and selectivity are dominated by the choice of metal of MPcs and are further modulated by heteroatomic linkages. Comparison tests on metal-free phthalocyanine MOF analogs verified the dominant catalytic role of the central metal of the phthalocyanine over Cu nodes. DFT calculations suggested that, compared with the NiPc-based and NH-linked MOFs, CoPc-based and O-linked MOFs can lower the activation energies in the formation of carboxyl intermediate, thus giving higher activities and selectivity. These results highlighted the great modular tunability of the activity and selectivity of the catalytic performance of MOFs through the judicious design and choice of functional ligands.

High current densities (j=–13.1 mA cm^{-2} for **CoPc-Cu-O**:CB=1:0.5, and j=–17.3 mA cm^{-2} for **CoPc-Cu-O**:CB=1:1) with good selectivity toward CO product (FE_{CO} up to 85%) at a relatively low overpotential of –0.63 V can be achieved, which is one of best cathode materials for the catalytic electrochemical conversion of CO_2 to CO using reticular framework materials and is also comparable or better than composite materials made of MPc and conductive additives (e.g, CNT, CB, see **Table S11** for detailed comparison). Due to the good conductivity, **CoPc-Cu-O** electrodes without any conductive additive was able to achieve a current density of –9.5 mA cm^{-2} and a good FE_{CO} of 79%, which is currently the best performance compared with other systems that apply reticular frameworks as the only active materials without the addition of any conductive binders.

Our work demonstrates the high promise of the utilization of porous conductive MOFs for the electrochemical conversion of CO_2 to CO, and paves the way for the design of the high-performance CO_2 reduction catalysts through modular engineering by strategically approaching the optimal combinations of multifaceted structural factors, such as active metal sites, peripheral groups, and secondary sites. Even with low ratios of electroactive MPc sites on the fabricated electrodes, the current systems can still achieve higher TOF values (1.15 and 0.63 s^{-1} for **CoPc-Cu-NH** and **CoPc-Cu-O**, respectively, see **Table S10**) compared to other related framework systems. We anticipate that building upon the fundamental insight into the structure–property relationships of 2D framework materials reported herein, while exploring controlled growth of thin-films of conductive framework materials on electrode surfaces, optimization of the chemical composition of the conductive binder, and the use of strategic devices architectures relying on flow chemistry can lead to significant improvements of catalytic activity and selectivity in electrocatalysis in the future.

ASSOCIATED CONTENT

Supporting Information. The Supporting Information is available free of charge on the ACS Publications website.
Synthetic details, characterization, and conductivity measurements, electrochemical tests, and computational studies (PDF).

AUTHOR INFORMATION

Corresponding Author

katherine.a.mirica@dartmouth.edu

weiyang.li@dartmouth.edu

Author Contributions

†Z.M. and J.L. contributed equally to this work.

Notes

The authors declare no competing financial interests.

ACKNOWLEDGMENT

We acknowledge support from startup funds provided by Dartmouth College, from the Walter and Constance Burke Research Initiation Award, Army Research Office Young Investigator Program Grant No. W911NF-17-1-0398, National Science Foundation EPSCoR award (#1757371), Sloan Research Fellowship (FG-2018-10561), Cottrell Scholar Award (#26019), NSF CAREER Award (#1945219), US Army Cold Regions Research and Engineering Lab (Award No. W913E519C0008), 3M Non-Tenured Faculty Award, and Arthur L. Irving Institute for Energy and Society at Dartmouth. The authors thank the University Instrumentation Center at the University of New Hampshire (Durham, NH) for the access of XPS and SEM.

REFERENCES

1. Kumar, B.; Llorente, M.; Froehlich, J.; Dang, T.; Sathrum, A.; Kubiak, C. P. Photochemical and Photoelectrochemical Reduction of CO_2. *Annu. Rev. Phys. Chem.* **2012,** *63*, 541-569.
2. Appel, A. M.; Bercaw, J. E.; Bocarsly, A. B.; Dobbek, H.; DuBois, D. L.; Dupuis, M.; Ferry, J. G.; Fujita, E.; Hille, R.; Kenis, P. J.; Kerfeld, C. A.; Morris, R. H.; Peden, C. H.; Portis, A. R.; Ragsdale, S. W.; Rauchfuss, T. B.; Reek, J. N.; Seefeldt, L. C.; Thauer, R. K.; Waldrop, G. L. Frontiers, Opportunities, and Challenges in Biochemical and Chemical Catalysis of CO_2 Fixation. *Chem. Rev.* **2013,** *113*, 6621-6658.
3. Aresta, M.; Dibenedetto, A.; Angelini, A. Catalysis for the Valorization of Exhaust Carbon: From CO_2 to Chemicals, Materials, and Fuels. Technological Use of CO_2. *Chem. Rev.* **2014,** *114*, 1709-1742.
4. Ding, M.; Flaig, R. W.; Jiang, H. L.; Yaghi, O. M. Carbon Capture and Conversion Using Metal–Organic Frameworks and Mof-Based Materials. *Chem. Soc. Rev.* **2019,** *48*, 2783-2828.
5. Costentin, C.; Robert, M.; Saveant, J. M. Catalysis of the Electrochemical Reduction of Carbon Dioxide. *Chem. Soc. Rev.* **2013,** *42*, 2423-2436.
6. Fisher, B. J.; Eisenberg, R. Electrocatalytic Reduction of Carbon Dioxide by Using Macrocycles of Nickel and Cobalt. *J. Am. Chem. Soc.* **1980,** *102*, 7361-7363.
7. Saveant, J. M. Molecular Catalysis of Electrochemical Reactions. Mechanistic Aspects. *Chem. Rev.* **2008,** *108*, 2348-2378.
8. Benson, E. E.; Kubiak, C. P.; Sathrum, A. J.; Smieja, J. M. Electrocatalytic and Homogeneous Approaches to Conversion of CO_2 to Liquid Fuels. *Chem. Soc. Rev.* **2009,** *38*, 89-99.
9. Hawecker, J.; Lehn, J.-M.; Ziessel, R. Electrocatalytic Reduction of Carbon Dioxide Mediated by $Re(Bipy)(CO)_3Cl$ (Bipy = 2,2'-Bipyridine). *J. Chem. Soc., Chem. Commun.* **1984**, 328-330.
10. Beley, M.; Collin, J. P.; Ruppert, R.; Sauvage, J. P. Electrocatalytic Reduction of Carbon Dioxide by Nickel $Cyclam^{2+}$ in Water: Study of the Factors Affecting the Efficiency and the Selectivity of the Process. *J. Am. Chem. Soc.* **1986,** *108*, 7461-7467.
11. Bourrez, M.; Molton, F.; Chardon-Noblat, S.; Deronzier, A. $[Mn(Bipyridyl)(CO)_3Br]$: An Abundant Metal Carbonyl Complex as Efficient Electrocatalyst for CO_2 Reduction. *Angew. Chem. Int. Ed.* **2011,** *50*, 9903-9906.
12. Francke, R.; Schille, B.; Roemelt, M. Homogeneously Catalyzed Electroreduction of Carbon Dioxide-Methods, Mechanisms, and Catalysts. *Chem. Rev.* **2018,** *118*, 4631-4701.
13. Qiao, J.; Liu, Y.; Hong, F.; Zhang, J. A Review of Catalysts for the Electroreduction of Carbon Dioxide to Produce Low-Carbon Fuels. *Chem. Soc. Rev.* **2014,** *43*, 631-675.
14. Chapovetsky, A.; Welborn, M.; Luna, J. M.; Haiges, R.; Miller, T. F., 3rd; Marinescu, S. C. Pendant Hydrogen-Bond Donors in Cobalt Catalysts Independently Enhance CO_2 Reduction. *ACS Cent. Sci.* **2018,** *4*, 397-404.
15. Morris, A. J.; Meyer, G. J.; Fujita, E. Molecular Approaches to the Photocatalytic Reduction of Carbon Dioxide for Solar Fuels. *Acc. Chem. Res.* **2009,** *42*, 1983-1994.
16. Costentin, C.; Drouet, S.; Robert, M.; Saveant, J. M. A Local Proton Source Enhances CO_2 Electroreduction to CO by a Molecular Fe Catalyst. *Science* **2012,** *338*, 90-94.
17. Costentin, C.; Passard, G.; Robert, M.; Saveant, J. M. Ultraefficient Homogeneous Catalyst for the CO_2-to-CO Electrochemical Conversion. *Proc. Natl. Acad. Sci. U.S.A.* **2014,** *111*, 14990-14994.
18. Chen, Y.; Li, C. W.; Kanan, M. W. Aqueous CO_2 Reduction at Very Low Overpotential on Oxide-Derived Au Nanoparticles. *J. Am. Chem. Soc.* **2012,** *134*, 19969-19972.
19. Kim, D.; Resasco, J.; Yu, Y.; Asiri, A. M.; Yang, P. D. Synergistic Geometric and Electronic Effects for Electrochemical Reduction of Carbon Dioxide Using Gold-Copper Bimetallic Nanoparticles. *Nat Commun* **2014,** *5*.
20. Li, F.; Chen, L.; Knowles, G. P.; MacFarlane, D. R.; Zhang, J. Hierarchical Mesoporous SnO_2 Nanosheets on Carbon Cloth: A Robust and Flexible Electrocatalyst for CO_2 Reduction with High Efficiency and Selectivity. *Angew. Chem. Int. Ed.* **2017,** *56*, 505-509.
21. Gao, S.; Sun, Z.; Liu, W.; Jiao, X.; Zu, X.; Hu, Q.; Sun, Y.; Yao, T.; Zhang, W.; Wei, S.; Xie, Y. Atomic Layer Confined Vacancies for Atomic-Level Insights into Carbon Dioxide Electroreduction. *Nat Commun* **2017,** *8*, 14503.
22. Asadi, M.; Kumar, B.; Behranginia, A.; Rosen, B. A.; Baskin, A.; Repnin, N.; Pisasale, D.; Phillips, P.; Zhu, W.; Haasch, R.; Klie, R. F.; Kral, P.; Abiade, J.; Salehi-Khojin, A. Robust Carbon Dioxide Reduction on Molybdenum Disulphide Edges. *Nat Commun* **2014,** *5*, 4470.
23. Asadi, M.; Kim, K.; Liu, C.; Addepalli, A. V.; Abbasi, P.; Yasaei, P.; Phillips, P.; Behranginia, A.; Cerrato, J. M.; Haasch, R.; Zapol, P.; Kumar, B.; Klie, R. F.; Abiade, J.; Curtiss, L. A.; Salehi-Khojin, A. Nanostructured Transition Metal Dichalcogenide Electrocatalysts for CO_2 Reduction in Ionic Liquid. *Science* **2016,** *353*, 467-470.
24. Xu, J. Q.; Li, X. D.; Liu, W.; Sun, Y. F.; Ju, Z. Y.; Yao, T.; Wang, C. M.; Ju, H. X.; Zhu, J. F.; Wei, S. Q.; Xie, Y. Carbon Dioxide Electroreduction into Syngas Boosted by a Partially Delocalized Charge in Molybdenum Sulfide Selenide Alloy Monolayers. *Angew. Chem. Int. Ed.* **2017,** *56*, 9121-9125.
25. Sreekanth, N.; Nazrulla, M. A.; Vineesh, T. V.; Sailaja, K.; Phani, K. L. Metal-Free Boron-Doped Graphene for Selective Electroreduction of Carbon Dioxide to Formic Acid/Formate. *Chem. Commun.* **2015,** *51*, 16061-16064.
26. Saravanan, K.; Gottlieb, E.; Keith, J. A. Nitrogen-Doped Nanocarbon Materials under Electroreduction Operating Conditions and Implications for Electrocatalysis of CO_2. *Carbon* **2017,** *111*, 859-866.
27. Choi, S.; Kim, C.; Suh, J. M.; Jang, H. W. Reduced Graphene Oxide - Based Materials for Electrochemical Energy Conversion Reactions. *Carbon Energy* **2019,** *1*, 85-108.
28. Leung, J. J.; Vigil, J. A.; Warnan, J.; Edwardes Moore, E.; Reisner, E. Rational Design of Polymers for Selective CO_2 Reduction Catalysis. *Angew. Chem. Int. Ed.* **2019,** *58*, 7697-7701.
29. Coskun, H.; Aljabour, A.; De Luna, P.; Farka, D.; Greunz, T.; Stifter, D.; Kus, M.; Zheng, X.; Liu, M.; Hassel, A. W.; Schofberger, W.; Sargent, E. H.; Sariciftci, N. S.; Stadler, P. Biofunctionalized Conductive Polymers Enable Efficient CO_2 Electroreduction. *Sci. Adv.* **2017,** *3*, e1700686.
30. Liu, Y.; McCrory, C. C. L. Modulating the Mechanism of Electrocatalytic CO_2 Reduction by Cobalt Phthalocyanine through Polymer Coordination and Encapsulation. *Nat Commun* **2019,** *10*, 1683.
31. Sun, Z.; Ma, T.; Tao, H.; Fan, Q.; Han, B. Fundamentals and Challenges of Electrochemical CO_2 Reduction Using Two-Dimensional Materials. *Chem* **2017,** *3*, 560-587.
32. Chai, G. L.; Guo, Z. X. Highly Effective Sites and Selectivity of Nitrogen-Doped Graphene/Cnt Catalysts for CO_2 Electrochemical Reduction. *Chem. Sci.* **2016,** *7*, 1268-1275.

33. Lei, F.; Liu, W.; Sun, Y.; Xu, J.; Liu, K.; Liang, L.; Yao, T.; Pan, B.; Wei, S.; Xie, Y. Metallic Tin Quantum Sheets Confined in Graphene toward High-Efficiency Carbon Dioxide Electroreduction. *Nat. Commun.* **2016,** *7*, 12697.
34. Su, P.; Iwase, K.; Nakanishi, S.; Hashimoto, K.; Kamiya, K. Nickel-Nitrogen-Modified Graphene: An Efficient Electrocatalyst for the Reduction of Carbon Dioxide to Carbon Monoxide. *Small* **2016,** *12*, 6083-6089.
35. Li, F.; Chen, L.; Xue, M.; Williams, T.; Zhang, Y.; MacFarlane, D. R.; Zhang, J. Towards a Better Sn: Efficient Electrocatalytic Reduction of CO_2 to Formate by Sn/SnS_2 Derived from SnS_2 Nanosheets. *Nano Energy* **2017,** *31*, 270-277.
36. Lu, X.; Tan, T. H.; Ng, Y. H.; Amal, R. Highly Selective and Stable Reduction of CO_2 to CO by a Graphitic Carbon Nitride/Carbon Nanotube Composite Electrocatalyst. *Chem.-Eur. J.* **2016,** *22*, 11991-11996.
37. Zhang, X.; Wu, Z.; Zhang, X.; Li, L.; Li, Y.; Xu, H.; Li, X.; Yu, X.; Zhang, Z.; Liang, Y.; Wang, H. Highly Selective and Active CO_2 Reduction Electrocatalysts Based on Cobalt Phthalocyanine/Carbon Nanotube Hybrid Structures. *Nat Commun* **2017,** *8*, 14675.
38. Sun, L.; Reddu, V.; Fisher, A. C.; Wang, X. Electrocatalytic Reduction of Carbon Dioxide: Opportunities with Heterogeneous Molecular Catalysts. *Energy Environ. Sci.* **2020,** *13*, 374-403.
39. Cao, Z.; Kim, D.; Hong, D.; Yu, Y.; Xu, J.; Lin, S.; Wen, X.; Nichols, E. M.; Jeong, K.; Reimer, J. A.; Yang, P.; Chang, C. J. A Molecular Surface Functionalization Approach to Tuning Nanoparticle Electrocatalysts for Carbon Dioxide Reduction. *J. Am. Chem. Soc.* **2016,** *138*, 8120-8125.
40. Khezri, B.; Fisher, A. C.; Pumera, M. CO_2 Reduction: The Quest for Electrocatalytic Materials. *J. Mater. Chem. A* **2017,** *5*, 8230-8246.
41. Verma, S.; Hamasaki, Y.; Kim, C.; Huang, W.; Lu, S.; Jhong, H.-R. M.; Gewirth, A. A.; Fujigaya, T.; Nakashima, N.; Kenis, P. J. A. Insights into the Low Overpotential Electroreduction of CO_2 to CO on a Supported Gold Catalyst in an Alkaline Flow Electrolyzer. *ACS Energy Lett.* **2017,** *3*, 193-198.
42. Zhang, W.; Hu, Y.; Ma, L.; Zhu, G.; Wang, Y.; Xue, X.; Chen, R.; Yang, S.; Jin, Z. Progress and Perspective of Electrocatalytic CO_2 Reduction for Renewable Carbonaceous Fuels and Chemicals. *Adv. Sci.* **2018,** *5*, 1700275.
43. Dinh, C.-T.; García de Arquer, F. P.; Sinton, D.; Sargent, E. H. High Rate, Selective, and Stable Electroreduction of CO_2 to CO in Basic and Neutral Media. *ACS Energy Lett.* **2018,** *3*, 2835-2840.
44. Yaghi, O. M.; O'Keeffe, M.; Ockwig, N. W.; Chae, H. K.; Eddaoudi, M.; Kim, J. Reticular Synthesis and the Design of New Materials. *Nature* **2003,** *423*, 705-714.
45. Rungtaweevoranit, B.; Diercks, C. S.; Kalmutzki, M. J.; Yaghi, O. M. Spiers Memorial Lecture: Progress and Prospects of Reticular Chemistry. *Faraday Discuss* **2017,** *201*, 9-45.
46. Jiang, J.; Zhao, Y.; Yaghi, O. M. Covalent Chemistry Beyond Molecules. *J. Am. Chem. Soc.* **2016**.
47. Yaghi, O. M. Reticular Chemistry-Construction, Properties, and Precision Reactions of Frameworks. *J. Am. Chem. Soc.* **2016,** *138*, 15507-15509.
48. Diercks, C. S.; Liu, Y.; Cordova, K. E.; Yaghi, O. M. The Role of Reticular Chemistry in the Design of CO_2 Reduction Catalysts. *Nat. Mater.* **2018,** *17*, 301-307.
49. Kornienko, N.; Zhao, Y.; Kley, C. S.; Zhu, C.; Kim, D.; Lin, S.; Chang, C. J.; Yaghi, O. M.; Yang, P. Metal–Organic Frameworks for Electrocatalytic Reduction of Carbon Dioxide. *J. Am. Chem. Soc.* **2015,** *137*, 14129-14135.
50. Yaghi, O. M.; Li, Q. Reticular Chemistry and Metal–Organic Frameworks for Clean Energy. *MRS Bulletin* **2011,** *34*, 682-690.
51. Downes, C. A.; Marinescu, S. C. Electrocatalytic Metal–Organic Frameworks for Energy Applications. *ChemSusChem* **2017,** *10*, 4374-4392.
52. Lee, J.; Farha, O. K.; Roberts, J.; Scheidt, K. A.; Nguyen, S. T.; Hupp, J. T. Metal–Organic Framework Materials as Catalysts. *Chem. Soc. Rev.* **2009,** *38*, 1450-1459.
53. Zhang, T.; Lin, W. Metal–Organic Frameworks for Artificial Photosynthesis and Photocatalysis. *Chem. Soc. Rev.* **2014,** *43*, 5982-5993.
54. Farha, O. K.; Eryazici, I.; Jeong, N. C.; Hauser, B. G.; Wilmer, C. E.; Sarjeant, A. A.; Snurr, R. Q.; Nguyen, S. T.; Yazaydin, A. O.; Hupp, J. T. Metal–Organic Framework Materials with Ultrahigh Surface Areas: Is the Sky the Limit? *J. Am. Chem. Soc.* **2012,** *134*, 15016-15021.
55. Deng, H.; Grunder, S.; Cordova, K. E.; Valente, C.; Furukawa, H.; Hmadeh, M.; Gandara, F.; Whalley, A. C.; Liu, Z.; Asahina, S.; Kazumori, H.; O'Keeffe, M.; Terasaki, O.; Stoddart, J. F.; Yaghi, O. M. Large-Pore Apertures in a Series of Metal–Organic Frameworks. *Science* **2012,** *336*, 1018-1023.
56. Dong, B.-X.; Qian, S.-L.; Bu, F.-Y.; Wu, Y.-C.; Feng, L.-G.; Teng, Y.-L.; Liu, W.-L.; Li, Z.-W. Electrochemical Reduction of CO_2 to CO by a Heterogeneous Catalyst of Fe–Porphyrin-Based Metal–Organic Framework. *ACS Appl. Energy Mater.* **2018,** *1*, 4662-4669.
57. Kusama, S.; Saito, T.; Hashiba, H.; Sakai, A.; Yotsuhashi, S. Crystalline Copper(II) Phthalocyanine Catalysts for Electrochemical Reduction of Carbon Dioxide in Aqueous Media. *ACS Cata.* **2017,** *7*, 8382-8385.
58. Diercks, C. S.; Lin, S.; Kornienko, N.; Kapustin, E. A.; Nichols, E. M.; Zhu, C.; Zhao, Y.; Chang, C. J.; Yaghi, O. M. Reticular Electronic Tuning of Porphyrin Active Sites in Covalent Organic Frameworks for Electrocatalytic Carbon Dioxide Reduction. *J. Am. Chem. Soc.* **2018,** *140*, 1116-1122.
59. Matheu, R.; Gutierrez-Puebla, E.; Monge, M. A.; Diercks, C. S.; Kang, J.; Prevot, M. S.; Pei, X.; Hanikel, N.; Zhang, B.; Yang, P.; Yaghi, O. M. Three-Dimensional Phthalocyanine Metal-Catecholates for High Electrochemical Carbon Dioxide Reduction. *J. Am. Chem. Soc.* **2019,** *141*, 17081-17085.
60. Wang, Y. R.; Huang, Q.; He, C. T.; Chen, Y.; Liu, J.; Shen, F. C.; Lan, Y. Q. Oriented Electron Transmission in Polyoxometalate-Metalloporphyrin Organic Framework for Highly Selective Electroreduction of CO_2. *Nat Commun* **2018,** *9*, 4466.
61. Lin, S.; Diercks, C. S.; Zhang, Y. B.; Kornienko, N.; Nichols, E. M.; Zhao, Y.; Paris, A. R.; Kim, D.; Yang, P.; Yaghi, O. M.; Chang, C. J. Covalent Organic Frameworks Comprising Cobalt Porphyrins for Catalytic CO_2 Reduction in Water. *Science* **2015,** *349*, 1208-1213.
62. Johnson, E. M.; Haiges, R.; Marinescu, S. C. Covalent-Organic Frameworks Composed of Rhenium Bipyridine and Metal Porphyrins: Designing Heterobimetallic Frameworks with Two Distinct Metal Sites. *ACS Appl. Mater. Interfaces* **2018,** *10*, 37919-37927.
63. Zhong, H.; Ghorbani-Asl, M.; Ly, K. H.; Zhang, J.; Ge, J.; Wang, M.; Liao, Z.; Makarov, D.; Zschech, E.; Brunner, E.; Weidinger, I. M.; Zhang, J.; Krasheninnikov, A. V.; Kaskel, S.; Dong, R.; Feng, X. Synergistic Electroreduction of Carbon Dioxide to Carbon Monoxide on Bimetallic Layered Conjugated Metal–Organic Frameworks. *Nat Commun* **2020,** *11*, 1409.
64. Hod, I.; Sampson, M. D.; Deria, P.; Kubiak, C. P.; Farha, O. K.; Hupp, J. T. Fe-Porphyrin-Based Metal–Organic Framework Films as High-Surface Concentration, Heterogeneous Catalysts for Electrochemical Reduction of CO_2. *ACS Cata.* **2015,** *5*, 6302-6309.
65. Jiang, D.; Huang, N.; Lee, K. H.; Irle, S.; Jiang, Q.; Yue, Y.; Xu, X. A Stable and Conductive Metallophthalocyanine Framework for Electrocatalytic Carbon Dioxide Reduction in Water. *Angew. Chem. Int. Ed.* **2020,** *59*, 16587-16593
66. Guo, J.; Xu, Y.; Jin, S.; Chen, L.; Kaji, T.; Honsho, Y.; Addicoat, M. A.; Kim, J.; Saeki, A.; Ihee, H.; Seki, S.; Irle, S.; Hiramoto, M.; Gao, J.; Jiang, D. Conjugated Organic Framework with Three-Dimensionally Ordered Stable Structure and Delocalized π Clouds. *Nat. Commun.* **2013,** *4*, 2736.
67. Sun, L.; Campbell, M. G.; Dincă, M. Electrically Conductive Porous Metal–Organic Frameworks. *Angew. Chem. Int. Ed.* **2016,** *55*, 3566-3579.
68. Ko, M.; Mendecki, L.; Mirica, K. A. Conductive Two-Dimensional Metal–Organic Frameworks as Multifunctional Materials. *Chem. Commun.* **2018,** *54*, 7873-7891.
69. Kim, S.; Choi, H. C. Light-Promoted Synthesis of Highly-Conjugated Crystalline Covalent Organic Framework. *Nat. Commun.* **2019,** *2,* 60.
70. Wang, M.; Ballabio, M.; Wang, M.; Lin, H. H.; Biswal, B. P.; Han, X.; Paasch, S.; Brunner, E.; Liu, P.; Chen, M.; Bonn, M.; Heine, T.; Zhou, S.; Canovas, E.; Dong, R.; Feng, X. Unveiling Electronic Properties in Metal-Phthalocyanine-Based Pyrazine-Linked Conjugated Two-Dimensional Covalent Organic Frameworks. *J. Am. Chem. Soc.* **2019,** *141,* 16810–16816.
71. Meng, Z.; Stolz, R. M.; Mirica, K. A. Two-Dimensional Chemiresistive Covalent Organic Framework with High Intrinsic Conductivity. *J. Am. Chem. Soc.* **2019,** *141*, 11929-11937.
72. Xie, L. S.; Skorupskii, G.; Dinca, M. Electrically Conductive Metal–Organic Frameworks. *Chem. Rev.* **2020,** *120*, 8536–8580.

73. Wang, M.; Torbensen, K.; Salvatore, D.; Ren, S.; Joulie, D.; Dumoulin, F.; Mendoza, D.; Lassalle-Kaiser, B.; Isci, U.; Berlinguette, C. P.; Robert, M. Co2 Electrochemical Catalytic Reduction with a Highly Active Cobalt Phthalocyanine. *Nat. Commun.* **2019,** *10*, 3602.

74. Han, B.; Ou, X.; Deng, Z.; Song, Y.; Tian, C.; Deng, H.; Xu, Y. J.; Lin, Z. Nickel Metal–Organic Framework Monolayers for Photoreduction of Diluted CO_2: Metal-Node-Dependent Activity and Selectivity. *Angew. Chem. Int. Ed.* **2018,** *57*, 16811-16815.

75. Azcarate, I.; Costentin, C.; Robert, M.; Saveant, J. M. Through-Space Charge Interaction Substituent Effects in Molecular Catalysis Leading to the Design of the Most Efficient Catalyst of CO_2-to-CO Electrochemical Conversion. *J. Am. Chem. Soc.* **2016,** *138*, 16639-16644.

76. Hmadeh, M.; Lu, Z.; Liu, Z.; Gándara, F.; Furukawa, H.; Wan, S.; Augustyn, V.; Chang, R.; Liao, L.; Zhou, F.; Perre, E.; Ozolins, V.; Suenaga, K.; Duan, X.; Dunn, B.; Yamamto, Y.; Terasaki, O.; Yaghi, O. M. New Porous Crystals of Extended Metal-Catecholates. *Chem. Mater.* **2012,** *24*, 3511-3513.

77. Meng, Z.; Aykanat, A.; Mirica, K. A. Welding Metallophthalocyanines into Bimetallic Molecular Meshes for Ultrasensitive, Low-Power Chemiresistive Detection of Gases. *J. Am. Chem. Soc.* **2019,** *141*, 2046-2053.

78. Weng, Z.; Wu, Y.; Wang, M.; Jiang, J.; Yang, K.; Huo, S.; Wang, X. F.; Ma, Q.; Brudvig, G. W.; Batista, V. S.; Liang, Y.; Feng, Z.; Wang, H. Active Sites of Copper-Complex Catalytic Materials for Electrochemical Carbon Dioxide Reduction. *Nat. Commun.* **2018,** *9*, 415.

79. Zhang, Z.; Xiao, J.; Chen, X. J.; Yu, S.; Yu, L.; Si, R.; Wang, Y.; Wang, S.; Meng, X.; Wang, Y.; Tian, Z. Q.; Deng, D. Reaction Mechanisms of Well-Defined Metal-N_4 Sites in Electrocatalytic CO_2 Reduction. *Angew. Chem. Int. Ed.* **2018,** *57*, 16339-16342.

80. Tan, X.; Yu, C.; Zhao, C.; Huang, H.; Yao, X.; Han, X.; Guo, W.; Cui, S.; Huang, H.; Qiu, J. Restructuring of Cu_2O to Cu_2O@Cu-Metal–Organic Frameworks for Selective Electrochemical Reduction of CO_2. *ACS Appl. Mater. Interfaces* **2019,** *11*, 9904-9910.

81. Basova, T. V.; Kiselev, V. G.; Schuster, B.-E.; Peisert, H.; Chassé, T. Experimental and Theoretical Investigation of Vibrational Spectra of Copper Phthalocyanine: Polarized Single-Crystal Raman Spectra, Isotope Effect and Dft Calculations. *J. Raman Spectrosc.* **2009,** *40*, 2080-2087.

82. Jia, H.; Yao, Y.; Zhao, J.; Gao, Y.; Luo, Z.; Du, P. A Novel Two-Dimensional Nickel Phthalocyanine-Based Metal–Organic Framework for Highly Efficient Water Oxidation Catalysis. *J. Mater. Chem. A* **2018,** *6*, 1188-1195.

83. Plenge, T.; Dillinger, R.; Santagostini, L.; Casella, L.; Tuczek, F. Catecholate Adducts of Binuclear Copper Complexes Modelling the Type 3 Copper Active Site— Spectroscopic Characterization and Relevance to the Tyrosinase Reaction. *Z. Anorg. Allg. Chem* **2003,** *629*, 2258-2265.

84. Koval, I. A.; Gamez, P.; Belle, C.; Selmeczi, K.; Reedijk, J. Synthetic Models of the Active Site of Catechol Oxidase: Mechanistic Studies. *Chem. Soc. Rev.* **2006,** *35*, 814-840.

85. Miner, E. M.; Wang, L.; Dinca, M. Modular O_2 Electroreduction Activity in Triphenylene-Based Metal–Organic Frameworks. *Chem. Sci.* **2018,** *9*, 6286-6291.

86. Wu, S.; Wen, G.; Schlogl, R.; Su, D. S. Carbon Nanotubes Oxidized by a Green Method as Efficient Metal-Free Catalysts for Nitroarene Reduction. *Phys. Chem. Chem. Phys.* **2015,** *17*, 1567-1571.

87. Qi, W.; Liu, W.; Zhang, B.; Gu, X.; Guo, X.; Su, D. Oxidative Dehydrogenation on Nanocarbon: Identification and Quantification of Active Sites by Chemical Titration. *Angew. Chem. Int. Ed.* **2013,** *52*, 14224-14228.

88. Campbell, M. G.; Sheberla, D.; Liu, S. F.; Swager, T. M.; Dincă, M. Cu_3(Hexaiminotriphenylene)$_2$: An Electrically Conductive 2D Metal–Organic Framework for Chemiresistive Sensing. *Angew. Chem. Int. Ed.* **2015,** *54*, 4349-4352.

89. Yang, C.; Dong, R.; Wang, M.; Petkov, P. S.; Zhang, Z.; Wang, M.; Han, P.; Ballabio, M.; Brauninger, S. A.; Liao, Z.; Zhang, J.; Schwotzer, F.; Zschech, E.; Klauss, H. H.; Canovas, E.; Kaskel, S.; Bonn, M.; Zhou, S.; Heine, T.; Feng, X. A Semiconducting Layered Metal–Organic Framework Magnet. *Nat. Commun.* **2019,** *10*, 3260.

90. Nagatomi, H.; Yanai, N.; Yamada, T.; Shiraishi, K.; Kimizuka, N. Synthesis and Electric Properties of a Two-Dimensional Metal–Organic Framework Based on Phthalocyanine. *Chem.-Eur. J.* **2018,** *24*, 1806-1810.

91. Dou, J. H.; Sun, L.; Ge, Y.; Li, W.; Hendon, C. H.; Li, J.; Gul, S.; Yano, J.; Stach, E. A.; Dincă, M. Signature of Metallic Behavior in the Metal–Organic Frameworks M_3(Hexaiminobenzene)$_2$ (M = Ni, Cu). *J. Am. Chem. Soc.* **2017,** *139*, 13608–13611.

92. Feng, D.; Lei, T.; Lukatskaya, M. R.; Park, J.; Huang, Z.; Lee, M.; Shaw, L.; Chen, S.; Yakovenko, A. A.; Kulkarni, A.; Xiao, J.; Fredrickson, K.; Tok, J. B.; Zou, X.; Cui, Y.; Bao, Z. Robust and Conductive Two-Dimensional Metal–Organic Frameworks with Exceptionally High Volumetric and Areal Capacitance. *Nat. Energy* **2018,** *3*, 30-36.

93. Sheberla, D.; Bachman, J. C.; Elias, J. S.; Sun, C. J.; Shao-Horn, Y.; Dincă, M. Conductive Mof Electrodes for Stable Supercapacitors with High Areal Capacitance. *Nat. Mater.* **2016,** *16*, 220-225.

94. Park, J.; Lee, M.; Feng, D.; Huang, Z.; Hinckley, A. C.; Yakovenko, A.; Zou, X.; Cui, Y.; Bao, Z. Stabilization of Hexaaminobenzene in a 2D Conductive Metal–Organic Framework for High Power Sodium Storage. *J. Am. Chem. Soc.* **2018,** *140*, 10315-10323.

95. Yao, M.-S.; Lv, X.-J.; Fu, Z.-H.; Li, W.-H.; Deng, W.-H.; Wu, G.-D.; Xu, G. Layer-by-Layer Assembled Conductive Metal–Organic Framework Nanofilms for Room-Temperature Chemiresistive Sensing. *Angew. Chem. Int. Ed.* **2017,** *129*, 16737-16741.

96. Kambe, T.; Sakamoto, R.; Kusamoto, T.; Pal, T.; Fukui, N.; Hoshiko, K.; Shimojima, T.; Wang, Z.; Hirahara, T.; Ishizaka, K.; Hasegawa, S.; Liu, F.; Nishihara, H. Redox Control and High Conductivity of Nickel Bis(Dithiolene) Complex π-Nanosheet: A Potential Organic Two-Dimensional Topological Insulator. *J. Am. Chem. Soc.* **2014,** *136*, 14357-14360.

97. Clough, A. J.; Skelton, J. M.; Downes, C. A.; de la Rosa, A. A.; Yoo, J. W.; Walsh, A.; Melot, B. C.; Marinescu, S. C. Metallic Conductivity in a Two-Dimensional Cobalt Dithiolene Metal–Organic Framework. *J. Am. Chem. Soc.* **2017,** *139*, 10863-10867.

98. Xu, Z.; Wong, Y. L.; Xiao, R.; Hou, Y., Electronic and Ionic Conductivity of Metal–Organic Frameworks. In *Comprehensive Supramolecular Chemistry II*, 2017; pp 399-423.

99. Le Moigne, J.; Even, R. Spectroscopic Properties and Conductivity of Thin Films of Partially Reduced Metallo-Phthalocyanines. *J. Chem. Phys.* **1985,** *83*, 6472-6479.

100. Kutzler, F. W.; Barger, W. R.; Snow, A. W.; Wohltjen, H. An Investigation of Conductivity in Metal-Substituted Phthalocyanine Langmuir-Blodgett Films. *Thin Solid Films* **1987,** *155*, 1-16.

101. Claessens, C. G.; Hahn, U.; Torres, T. Phthalocyanines: From Outstanding Electronic Properties to Emerging Applications. *Chem. Rec.* **2008,** *8*, 75-97.

102. Liu, J.; Fan, Y. Z.; Li, X.; Xu, Y. W.; Zhang, L.; Su, C. Y. Catalytic Space Engineering of Porphyrin Metal–Organic Frameworks for Combined CO_2 Capture and Conversion at a Low Concentration. *ChemSusChem* **2018,** *11*, 2340-2347.

103. Liang, L.; Liu, C.; Jiang, F.; Chen, Q.; Zhang, L.; Xue, H.; Jiang, H. L.; Qian, J.; Yuan, D.; Hong, M. Carbon Dioxide Capture and Conversion by an Acid-Base Resistant Metal–Organic Framework. *Nat Commun* **2017,** *8*, 1233.

104. Ding, M.; Jiang, H.-L. Incorporation of Imidazolium-Based Poly(Ionic Liquid)s into a Metal–Organic Framework for CO_2 Capture and Conversion. *ACS Cata.* **2018,** *8*, 3194-3201.

105. Wang, Y.; Huang, N. Y.; Shen, J. Q.; Liao, P. Q.; Chen, X. M.; Zhang, J. P. Hydroxide Ligands Cooperate with Catalytic Centers in Metal–Organic Frameworks for Efficient Photocatalytic CO_2 Reduction. *J. Am. Chem. Soc.* **2018,** *140*, 38-41.

106. Wu, Y.; Jiang, Z.; Lu, X.; Liang, Y.; Wang, H. Domino Electroreduction of CO_2 to Methanol on a Molecular Catalyst. *Nature* **2019,** *575*, 639-642.

107. Russell, P. G. The Electrochemical Reduction of Carbon Dioxide, Formic Acid, and Formaldehyde. *J. Electrochem. Soc.* **1977,** *124*.

108. Bandi, A. Electrochemical Reduction of Carbon Dioxide on Conductive Metallic Oxides. *J. Electrochem. Soc.* **1990,** *137*.

109. Kuhl, K. P.; Cave, E. R.; Abram, D. N.; Jaramillo, T. F. New Insights into the Electrochemical Reduction of Carbon Dioxide on Metallic Copper Surfaces. *Energy Environ. Sci.* **2012,** *5*.

110. Hatsukade, T.; Kuhl, K. P.; Cave, E. R.; Abram, D. N.; Jaramillo, T. F. Insights into the Electrocatalytic Reduction of CO_2 on Metallic Silver Surfaces. *Phys. Chem. Chem. Phys.* **2014,** *16*, 13814-13819.

111. Ye, L.; Liu, J.; Gao, Y.; Gong, C.; Addicoat, M.; Heine, T.; Wöll, C.; Sun, L. Highly Oriented Mof Thin Film-Based Electrocatalytic Device for the Reduction of CO_2 to CO Exhibiting High Faradaic Efficiency. *J. Mater. Chem. A* **2016,** *4*, 15320-15326.

112. Zhao, C.; Dai, X.; Yao, T.; Chen, W.; Wang, X.; Wang, J.; Yang, J.; Wei, S.; Wu, Y.; Li, Y. Ionic Exchange of Metal–Organic Frameworks to Access Single Nickel Sites for Efficient Electroreduction of CO_2. *J. Am. Chem. Soc.* **2017,** *139*, 8078-8081.
113. Nitopi, S.; Bertheussen, E.; Scott, S. B.; Liu, X.; Engstfeld, A. K.; Horch, S.; Seger, B.; Stephens, I. E. L.; Chan, K.; Hahn, C.; Norskov, J. K.; Jaramillo, T. F.; Chorkendorff, I. Progress and Perspectives of Electrochemical CO_2 Reduction on Copper in Aqueous Electrolyte. *Chem. Rev.* **2019**.
114. Gottle, A. J.; Koper, M. T. M. Proton-Coupled Electron Transfer in the Electrocatalysis of CO_2 Reduction: Prediction of Sequential vs. Concerted Pathways Using DFT. *Chem. Sci.* **2017,** *8*, 458-465.
115. Han, N.; Wang, Y.; Ma, L.; Wen, J.; Li, J.; Zheng, H.; Nie, K.; Wang, X.; Zhao, F.; Li, Y.; Fan, J.; Zhong, J.; Wu, T.; Miller, D. J.; Lu, J.; Lee, S.-T.; Li, Y. Supported Cobalt Polyphthalocyanine for High-Performance Electrocatalytic CO_2 Reduction. *Chem* **2017,** *3*, 652-664.
116. Nielsen, I. M.; Leung, K. Cobalt-Porphyrin Catalyzed Electrochemical Reduction of Carbon Dioxide in Water. 1. A Density Functional Study of Intermediates. *J. Phys. Chem. A* **2010,** *114*, 10166-10173.
117. Shen, J.; Kolb, M. J.; Göttle, A. J.; Koper, M. T. M. Dft Study on the Mechanism of the Electrochemical Reduction of CO_2 Catalyzed by Cobalt Porphyrins. *J. Phys. Chem. C* **2016,** *120*, 15714-15721.
118. Hansen, H. A.; Varley, J. B.; Peterson, A. A.; Norskov, J. K. Understanding Trends in the Electrocatalytic Activity of Metals and Enzymes for CO_2 Reduction to CO. *J. Phys. Chem. Lett.* **2013,** *4*, 388-392.

Insert Table of Contents artwork here